FLUORESCENCE STUDY OF THE DIVALENT CATION-TRANSPORT MECHANISM OF IONOPHORE A23187 IN PHOSPHOLIPID MEMBRANES

MICHAEL A. KOLBER AND DUNCAN H. HAYNES, *Department of Pharmacology, University of Miami School of Medicine Miami, Florida 33101*

ABSTRACT The mechanism for transport of divalent cations across phospholipid bilayers by the ionophore A23187 was investigated. The intrinsic fluorescence of the ionophore was used in equilibrium and rapid-mixing experiments as an indicator of ionophore environment and complexation with divalent cations. The neutral (protonated) form of the ionophore binds strongly to the membrane, with a high quantum yield relative to that in the aqueous phase. The negatively charged form of the ionophore binds somewhat less strongly, with a lower quantum yield, and does not move across the membrane. Complexation of the negatively charged form with divalent cations was measured by the decrease in fluorescence. An apparent rate constant (k_{app}) for transport of the ionophore across the membrane was determined from the rate of fluorescence changes observed in stopped-flow rapid kinetic experiments. The variation of k_{app} was studied as a function of pH, temperature, ionophore concentration, membrane lipid composition, and divalent cation concentration and type. Analysis and comparison with equilibrium constants for protonation and complexation show that A23187 and its metal:ionophore complexes bind near the membrane-water interface in the lipid polar-head region. The interfacial reactions occur rapidly, compared with the transmembrane reactions, and are thus in equilibrium during transport. The transport cycle can be described as follows: a 1:1 complex is formed between the membrane bound $A23187^-(A_m^-)$ and the aqueous divalent cation with dissociation constant $K_1 \sim 4.6 \times 10^{-4}$ M. This is in equilibrium with a 1:2 (metal:ionophore) complex ($K_2 \sim 3.0 \times 10^{-4}$ [ionophore/lipid]) that is responsible for transporting the divalent cations across the membrane. The rate constant for translocation of the 1:2 complex is 0.1–0.3 s^{-1}. Dissociation of the complex of the *trans* side and protonation occur rapidly. The rate constant for translocation of $H^+ \cdot A23187^-$ is 28 s^{-1}. A theory is presented that is capable of reproducing the kinetic data at any calcium concentration. The cation specificity for ionophore complex transport (k_{app}), determined at low ionophore concentration for a series of divalent cations, was found to be proportional to the equilibrium constant for 1:1 complexation. The order of ion specificity for these processes was found to be $Ca^{2+} > Mg^{2+} > Sr^{2+} > Ba^{2+}$. Interactions with Na^+ were not observed. Maximal values of k_{app} were observed for vesicles prepared from pure dimyristoyl phosphatidylcholine. Inclusion of phosphatidyl ethanolamine, phosphatidic acid, or dipalmatoyl phosphatidylcholine resulted in lower values of k_{app}. Calcium transport by A23187 is compared with that of X537A, and it is shown that the former is 67-fold faster. The difference in rates is due to differences in the ability of each ionophore to form a 1:2 complex from a 1:1 complex.

INTRODUCTION

The carboxylic ionophore A23187 is known to be highly selective for moving Ca^{2+} and Mg^{2+} across biological membranes (1). Although many studies have investigated equilibrium and steady-state properties in a number of systems (2–4), transport of these metal:ionophore

complexes has not yet been subjected to a detailed kinetic treatment. The present study uses the intrinsic fluorescence of the ionophore to determine the equilibrium and kinetic constants of the ionophore's transport cycle in phospholipid (PL) vesicle membranes.

The intrinsic fluorescence of A23187 has been shown to be a sensitive probe of the polarity of the ionophore's environment (2, 5, 6) and the state of complexation of divalent cations with the ionophore (6, 7). The fluorescence quantum yield increases with a decrease in solvent polarity and decreases with complexation. Work done in this laboratory has shown (8) that the intrinsic fluorescence of X537A, a less specific transporter of divalent cations than A23187, can be used to monitor cation transport across PL membranes. Equilibrium titrations that measure steady-state fluorescence were used in conjunction with stopped flow rapid-mixing experiments to provide information on the stoichiometries of the transporting and nontransporting species. The equilibrium and rapid mixing experiments that were used to elucidate the mechanism of transport of cations by X537A have been extended to A23187 in the present work. A scheme for the mechanism of transport of divalent cations with A23187 is presented in Fig. 1. The interface region corresponds approximately to the polar head group and glycerol backbone region of the lipids. We show that the binding to the interface region and the complexation reactions are rapid (equilibrium) compared with the transmembrane reactions. This scheme is examined under various conditions and is treated quantitatively.

MATERIALS AND METHODS

The PL used were purchased as follows: from Sigma Chemical Co., St. Louis, Mo., dimyristoyl-L-α-phosphatidylcholine (DMPC) No. P-0888, dipalimitoyl-L-α-phosphatidylcholine (DPPC) No. P-0763, L-α-phosphatidyl-L-serine (PS) No. P-06641; from Calbiochem-Behring Corp., American Hoechst, San Diego, Calif., dimyristoyl-L-α-phosphatidylethanolamine (DMPE) No. 524634; and from

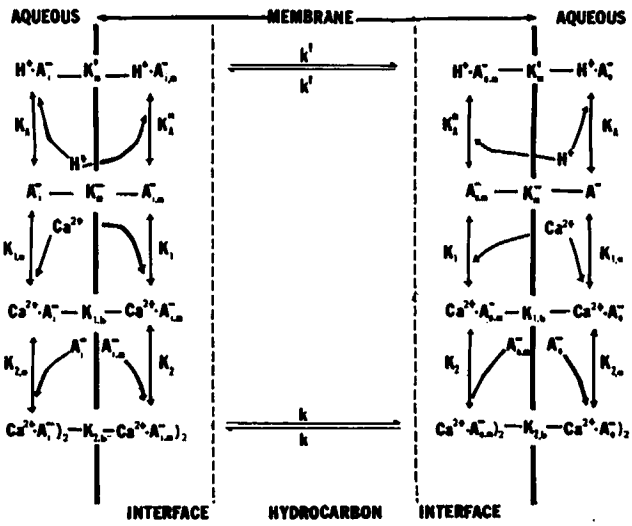

FIGURE 1 A schematic representation of the transport for the movement of A23187 (A) and its Ca^{2+} complexes is shown. The equilibrium association constants are defined by K and the rate constants by k. The subscripts "i" and "o" represent the inside and outside of the vesicle, respectively. The super- or subscript "m" indicates membrane bound. $(Ca^{2+} \cdot A^-)_2$ indicates two A^- complexed with one Ca^{2+}.

Koch-Light Laboratories Ltd., Colnbrook, Buckinghamshire, England, phosphatidic acid (PA; from egg lecithin) No. 63354. The carboxylic ionophore A23187 was purchased from Calbiochem-Behring Corp., lot No. 803577. All the lipids and ionophore that were used had a purity of >98% (stated purity) and were used without further purification.

The lipid vesicles were prepared by first dispersing 6 mg of lipid into 2 ml buffer (50 mM Hepes, 0.025 mM EDTA) by vortexing for 15 min and by 2 min of mild sonication. Small bilayer vesicles were subsequently prepared by ultrasonication of the lipid dispersion for 10 min at 37°C. A Heat Systems-Ultrasonics, Inc. (Plainview, N.Y.) W185D Sonifer at stage 5 (nominal output 60 W) with a titanium microtip was used to sonicate all samples. Using optical absorption, we did not observe any contamination by titanium particles after ultracentrifugation of sonicated buffer at 100,000 *g* for 20 min, compared with a solution that was not centrifuged. Maximum fluorescence of A23187 with vesicles in 50 mM Hepes (pH 7) could be obtained if 0.025 mM EDTA was added. Because EDTA is a chelator of multivalent cationic impurities (9) 0.25 mM EDTA was added to the stock vesicle solutions. All unsaturated lipids were dried and then sonicated under a nitrogen atmosphere to prevent oxidation. All experiments were completed within 2 h of the vesicle preparation.

It has been shown (10, 11) that ultrasonication produces small bilayer vesicles with only a small fraction (<5% lipid) existing in a heterogeneous (multilamellar, etc.) fraction. Therefore, no efforts were made to separate these two fractions since >95% of the observed signal are due to the small unilamellar vesicles. This assumption proved valid, as evidenced by the reproducibility of the apparent rate constant ($k_{app} = 0.51 \pm 0.22\ s^{-1}$, $n = 13$; see Results).

The equilibrium data for A23187 experiments were obtained on a Hitachi-Perkin Elmer MPF3 spectrofluorometer (Hitachi-Perkin Elmer Corp., Norwalk, Conn.) (excitation and emission at 380 and 440 nm, respectively). The spectral maxima of A23187 were virtually insensitive to variations in pH (from pH 2–7), additions of Ca^{2+}, and vesicle lipid composition. The sample cuvette volume was ~0.4 ml, with an optical path length of 0.5 cm. The CTC experiments (chlorotetracycline obtained from ICN K & K Laboratories Inc., Plainview, N.Y., No. 100235) were run on the same spectrofluoremeter (excitation and emission at 380 and 520 nm, respectively). The lipid vesicles were prepared as described and contained 1 mM Ca^{2+} and 0.1 mM CTC in a 0.1 M Hepes buffer at pH 7.0. The stock lipid concentration was 3 mg/ml (nominally determined) and diluted to 0.07 mg/ml in a solution containing 0.05 mM EDTA.

Rapid-mixing experiments were performed with an Aminco-Morrow stopped flow apparatus (Silver Spring, Md.; cat. No. 4-8409) in the fluorescence mode. The ionophore was excited with light at a wavelength of 380 nm and the fluorescence was collected after passing through a Schott GG 400-nm cut-off filter (Schott Optical Glass Inc., Duryea, Pa.). All vesicle solutions were prepared as described above. The final solution volumes were 6 ml, in which the stock lipid solution was diluted to 0.03 mg/ml (nominally determined), unless otherwise specified. The photomultiplier gains were not the same for each series of rapid-mixing experiments; comparison between the amplitudes could be made after normalization between experiments at a 0.33-mM Ca^{2+} concentration. The oscilloscope traces were digitized on the PROPHET computer system by a graphics tablet (see Acknowledgements). The system's curve-fitting package (a least-squares procedure) was used to obtain statistics and fit parameter values. Both equilibrium and kinetic experiments were run at 34°C unless otherwise specified.

RESULTS AND DISCUSSION

Equilibrium Studies

The equilibrium properties of A23187 in DMPC vesicles were studied with the aid of the ionophore's intrinsic fluorescence. In particular, we investigated the changes in fluorescence as a function of ionophore, lipid, hydrogen ion, and cation concentration to obtain the equilibrium association constants for the ionophore binding to the membrane and for complexation with various cations.

DEPENDENCE OF FLUORESCENCE ON IONOPHORE AND LIPID CONCENTRATONS Fig. 2 shows the change in fluorescence as a function of ionophore concentration for lipid concentrations of 0.073 and 0.029 mg/ml. At high ionophore concentrations the fluorescence change is not proportional to the concentration of A23187. To avoid any complications that might occur in the nonlinear region, all subsequent equilibrium experiments were performed in the linear region, where the fluorescence change is directly proportional to the ionophore concentration.

The fluorescence of A23187 in the aqueous phase was found to be small compared with the fluorescence in the membrane phase (fluorescence ratio <0.05 at all membrane concentrations used). This fact enabled us to use the ionophore's fluorescence as a direct measure of the ionophore binding in the membrane.[1] Fig. 3 shows the dependence of the change in fluorescence on the DMPC concentration. If the simple reaction scheme for ionophore binding to the membrane is assumed,

$$\text{A23187} + \text{membrane} \overset{K_B}{\longleftrightarrow} \text{A23187}_m, \tag{1}$$

where K_B is the apparent membrane association constant; and if we measure the membrane concentration as the concentration of PL, then the degree of binding can be expressed by the hyperbolic relationship

$$\frac{\Delta Fl}{\Delta Fl_{sat}} = \frac{[A23187]_m}{[A23187]_T} = \frac{K_B \cdot [PL]}{(1 + K_B \cdot [PL])}, \tag{2}$$

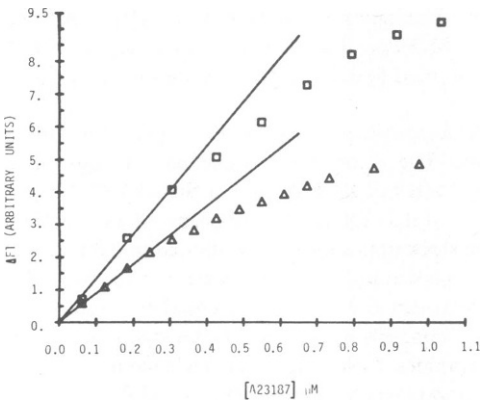

FIGURE 2

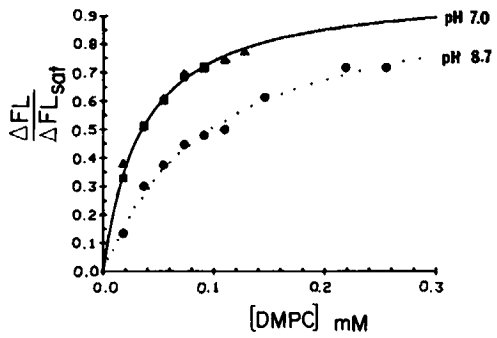

FIGURE 3

FIGURE 2 The fluorescence amplitude (in arbitrary units) is plotted against ionophore concentration for lipid (DMPC) concentrations of 0.073 mg/ml (□) and 0.029 mg/ml (△). The solid lines are drawn to indicate the region over which the fluorescence is proportional to the ionophore concentration.

FIGURE 3 The normalized change in fluorescence ($\Delta Fl/\Delta Fl_{sat}$) is plotted against lipid concentration for ionophore concentrations of 1.2×10^{-7} M (▲) and 2.5×10^{-7} (■) at pH 7.0, and at pH 8.7 (●) for ionophore concentrations of 2.5×10^{-7} M.

[1]The term "binding" is used here to indicate association of the ionophore with the membrane. Whether this association is due to a discrete and saturable binding site is not clear.

where $[A23187]_T$ is the total amount of ionophore, and ΔFl_{sat} is the maximum change in flourescence. This relationship can be used to fit the data in Fig. 3.

At a fixed pH (7.0), Fig. 3 shows that the binding of the ionophore on the membrane is independent of the ionophore concentration. At pH 8.7 the ionophore does not bind to the membrane as well as at pH 7.0. The solid and dotted lines in Fig. 3 are a least-squares fit to the data according to Eq. 2 with K_B values of $1.9 \times 10^4\ M^{-1}$ and $0.7 \times 10^4\ M^{-1}$, at pH 7.06 and 8.7, respectively. The ratio of the maximum fluorescence (ΔFl_{sat}) at pH 8.7 to ΔFl_{sat} at pH 7.0 was ~0.2 (data not shown). The dependence of K_B on $[H^+]$ shows that the neutral form of the ionophore binds better than the charged form in the membrane and has a higher fluorescence quantum yield.

DEPENDENCE OF FLUORESCENCE ON THE INTRINSIC EQUILIBRIUM CONSTANTS Fig. 4 shows a pH titration curve at constant lipid and ionophore concentrations. The apparent equilibrium association constant for protonation (K_A^{app}) from Fig. 4 is about -7.26. Our value for the pK_A is slightly higher than that found in earlier work (4), with egg phosphatidycholine (PC), in which an apparent pK_A of -6.7 was found.

The binding constants (K_B) and apparent equilibrium association constant for protonation (K_A^{app}) found from Figs. 3 and 4 depend explicitly on $[H^+]$ and lipid concentration, respectively. A more useful set of equilibrium constants are the intrinsic equilibrium constants. Fig. 1 shows that the appropriate constants include the binding constant of the neutral species (K_m^0), the association constant for protonation of the membrane species (K_A^m), the association constant for protonation of the aqueous species (K_A), and the membrane binding constant for the negative species, K_m^- ($= K_A K_m^0 / K_A^m$). The values for the intrinsic equilibrium constants can be obtained from the apparent constants if the fluorescence change is expressed as a function of the intrinsic constants. Since the fluorescence contribution of the ionophore in the aqueous phase is small, the total fluorescence change (ΔFl_T) is simply the sum of the negative ($[A_m^-]$) and neutral ($[A_m^0]$) forms,

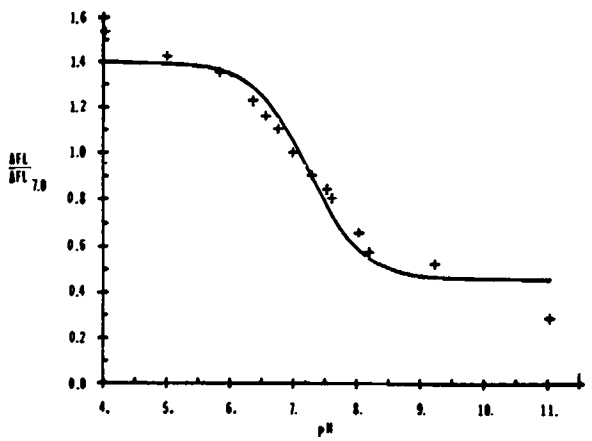

FIGURE 4 The fluorescence amplitude (normalized to 1.0) at pH 7.0 is plotted vs. pH. The solid line is a least-squares fit of Eq. 5 to the data; the equation was given by $\Delta Fl/\Delta Fl(pH = 7.0) = (1.41)(10^{(7.0-pH)} + 0.18)/(10^{(7.0-pH)} + 0.55)$. The concentration of DMPC was 1.73×10^{-4} M and $[A23187]_T = 2.5 \times 10^{-7}$ M.

$$\Delta Fl_T = \alpha[A_m^0] + \beta\,[A_m^-], \tag{3}$$

where α and β are the fluorescence contributions of the neutral and negative forms of the ionophore, respectively. With the conservation equation for the total amount of ionophore ($[A_T]$) it is straightforward to show that

$$[A_m^0] = \frac{K_A K_m^0 K_A^m\,[A_T] \cdot [H^+] \cdot [PL]}{(K_A K_m^0 K_A^m\,[H^+] \cdot [PL] + K_A K_m^0 \cdot [PL] + K_A K_A^m\,[H^+] + K_A^m)}, \tag{4a}$$

and

$$[A_m^-] = \frac{[A_m^0]}{[H^+] \cdot K_A^m}. \tag{4b}$$

Combining Eqs. 3, 4a, and b, we find that the total change in fluorescence is given by

$$\Delta Fl_T = \left(\alpha + \frac{\beta}{[H^+] \cdot K_A^m}\right) \left(\frac{K_A K_m^0 K_A^m\,[A_T][H^+][PL]}{K_A K_m^0 K_A^m [H^+] \cdot [PL] + K_A K_m^0\,[PL] + K_A K_A^m\,[H^+] + K_A^m}\right). \tag{5}$$

A comparison of Eq. 5 with 2 shows that the apparent binding constant K_B is given by

$$K_B = \frac{K_A K_m^0 K_A^m [H^+] + K_A K_m^0}{K_A K_A^m [H^+] + K_A^m}.$$

Similarly, we can show that the apparent equilibrium constant for protonation, K_A^{app}, is given by

$$K_A^{app} = \frac{K_A K_A^m + K_A K_m^0 K_A^m [PL]}{K_A^m + K_A K_m^0 [PL]}.$$

The estimated values for K_A, K_m^0 and K_A^m can be obtained when the values of K_B (pH = 7.0), and K_B (pH = 8.7) and the pK_A^{app} are used in the above equations. Table I gives the results of such an analysis. The value for the equilibrium association constant in the aqueous phase (−6.68) is in reasonable agreement with spin studies on PC bilayers (−6.3) (12). When Eq. 5 is used to fit Fig. 4 an additional result is that the neutral membrane-bound ionophore has approximately twice the quantum yield as the membrane-bound ionophore that is charged ($\beta/\alpha \simeq 0.55$).

TABLE I
EQUILIBRIUM CONSTANTS FOR A23187

Protonation		Membrane binding	
pK_A^m	pK_A	K_m^0	K_m
		(M^{-1})	(M^{-1})
−7.55	−6.68	4.9×10^4	6.61×10^3

The error in the fit constants for the curves in Fig. 3 was ~10%, whereas in Fig. 4 it was ~20%.

DETERMINATION OF DIVALENT CATION COMPLEXATION CONSTANTS It has been shown (5) that monovalent cations (Na^+, K^+, Li^+) complex poorly with A23187. We found that up to 50 mM Na^+ produced no decrease in the observed fluorescence, which is in accord with previous observations (5). It has been generally recognized, however, that divalent cations quench the ionophore's fluorescence (2, 6) by complexing with it. Furthermore, it has been shown (4) that Ca^{2+} complexation shifts the apparent pK_A in the pH titration curve to lower pH values. Since the binding affinity of A23187 for divalent cations is expected to be high we performed our experiments at pH 7 (near the pK_A^{app}), so that small Ca^{2+} additions would cause relatively large changes in binding and fluorescence. Fig. 5 shows the decrease in fluorescence (plotted positively) as a function of cation concentration. In agreement with earlier work (5, 13) we found that the affinity sequence for divalent cation-ionophore complexation follows $Ca^{2+} > Mg^{2+} > Sr^{2+} > Ba^{2+}$, with Ca^{2+} forming the strongest complex. If a 1:1 Ca^{2+}:ionophore complex is the dominant quenching species, the fluorescence should vary according to

$$\frac{\Delta Fl}{\Delta Fl_{max}} = \frac{K_{app}\,[M^{2+}]}{1 + K_{app}\,[M^{2+}]}, \tag{6}$$

which follows from the reaction

$$M^{2+} + A23187_m^- \overset{K_{app}}{\longleftrightarrow} M^{2+} - A23187_m^-, \tag{7}$$

where $[M^{2+}]$ is the aqueous divalent cation concentration, ΔFl_{max} is the maximum fluorescence change, and K_{app} is the apparent association constant for complexation. To verify that

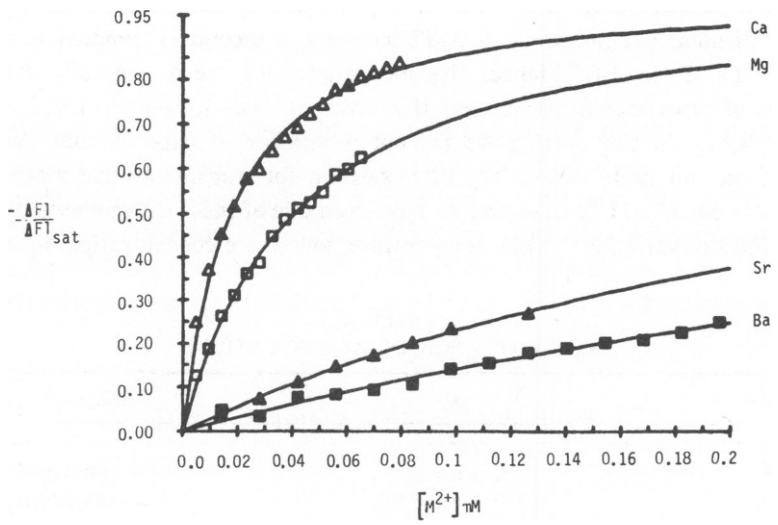

FIGURE 5 The decrease in the fluorescence (plotted positively) is shown vs. the concentration of divalent cation. The solid lines are the fit of Eq. 7 (text) to the data according to different values of K_{app} (Table II) for each cation. The lipid concentration was 1.73×10^{-4} M and ionophore concentration of 2.5×10^{-7} M.

quenching due to the formation of 1:2 (Ca^{2+}:ionophore) complexes was small compared with that of the 1:1 complexes we varied the ionophore concentration and investigated the effect on K_{app} of Ca^{2+}. If 1:2 complexes participated in the quenching of the ionophore's fluorescence to a significant extent, K_{app} would be roughly proportional to the ionophore concentration. We found that halving the ionophore concentration did not change K_{app} (~5% change), which indicates that 1:1 complexation was responsible for virtually all of the decrease in fluorescence.

As in the previous section, the apparent equilibrium association constant for complexation (K_{app}) can be related to the intrinsic 1:1 association constant (K_1) and the membrane binding constant of the 1:1 complex ($K_{1,B}$):

$$K_{app} = \left(\frac{K_1}{1 + K_A^{app}[H^+]}\right) \cdot \left(\frac{1 + \dfrac{1}{K_{1,B} \cdot [PL]}}{1 + \dfrac{1}{K_m^- [PL]}}\right).$$

We found that a fourfold decrease in PL concentration produced no change (<5%) in K_{app}, which indicates that the membrane binding constant for the negative species (K_m^-) and the membrane binding constant of the 1:1 complex ($K_{1,B}$) are approximately equal. Table II gives the values for K_1 (the intrinsic 1:1 association constant) and the maximal fluorescence change as compared with that when the complexing cation is Ca^{2+}. At infinite [Ca^{2+}] the fluorescence is totally quenched.

Kinetic Studies

Although a number of studies (1, 2, 4, 6, 14) have shown that A23187 facilitates movement of divalent cations across biological and PL membranes, the determination of the mechanism of transport of divalent cations using A23187 has been a secondary concern in most of this earlier work (1, 2, 6, 14). Hence, the mechanism has been generally inferred from consideration of experimental parameters that have not been fully interpreted in terms of a particular scheme. In this section we present a number of experimental methods, with analysis, that permit us to extract the rate constant for transmembrane movement of the Ca^{2+}:ionophore complex. Furthermore, we have used one of these experimental techniques to study the effects of variations in pH, temperature, ionophore concentration, lipid membrane

TABLE II
K_1 VALUES FOR DIVALENT CATIONS

Cation	K_1	$\Delta Fl_{max}/\Delta Fl_{max}^{Ca}$
	(M^{-1})	
Ca^{2+}	$1.56 \pm 0.8 \times 10^5$	1.0 ± 0.03
Mg^{2+}	$6.58 \pm 0.4 \times 10^4$	0.83 ± 0.06
Sr^{2+}	$8.02 \pm 1.2 \times 10^3$	0.89 ± 0.15
Ba^{2+}	$4.83 \pm 1.7 \times 10^3$	0.92 ± 0.36

The K_1 values were obtained by fitting Eq. 7 of the text to the points in Fig. 5. The values given are K_1 (see the Kinetic Studies section) and are related to K_{app} through $K_{app} = K_1/(1 + K_A^{app} \cdot [H^+])$, where $pK_A^{app} = -7.26$ (Fig. 4). ΔFl_{max}^{Ca} is the maximum change in Fl when the divalent cation is Ca^{2+}.

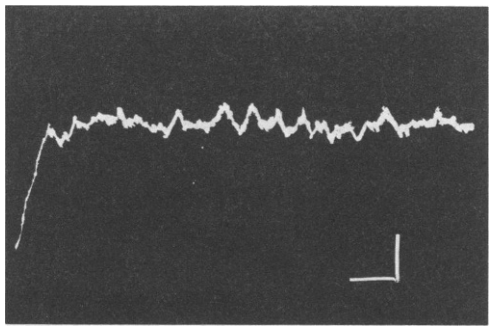

FIGURE 6 A stopped-flow progress curve showing the increase in fluorescence as a function of time is presented. The ordinate is fluorescence intensity given in units of voltage (50 mV/Div), and the abscissa in time after mixing (0.1 s/Div). Syringe *A* contained DMPC vesicles (0.06 mg/ml) in 0.01 M Hepes, pH 7.06; syringe *B* contained 6.7×10^{-8} M A23187 in 0.01 Hepes, pH 7.06. No divalent cations were present and the temperature was maintained at 34°C. The oscilloscope was set in the repetitive-sweep mode. The light-dark amplitude with water was 0.62 V.

composition, nature of the transported cation, and competition with X537A on ionophore mediated transport.

NATURE OF THE TRANSPORTING COMPLEXES A number of different experimental designs were used to separate out the components of ionophore transport that were due to the neutral ionophore complex ($H^+ \cdot A23187^-$) and the Ca^{2+}:ionophore complex. In the first experiment we were concerned with verifying that ionophore movement across the membrane

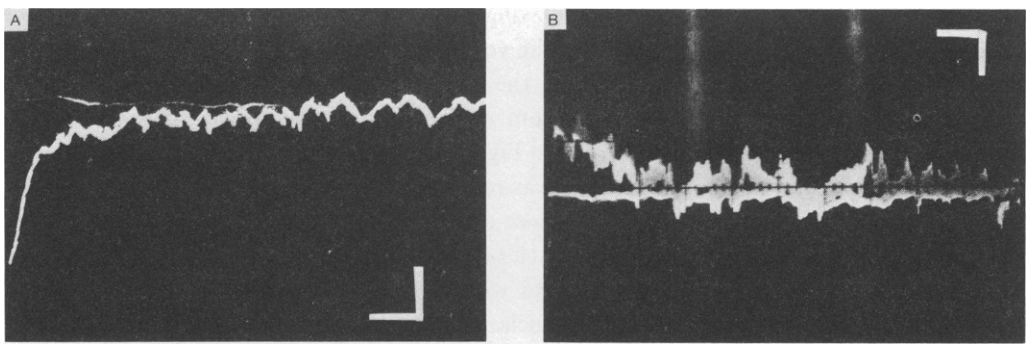

FIGURE 7 (*A*) A stopped-flow progress curve showing the effect of internal calcium on the fluorescence time-course is presented. The ordinate is fluorescence intensity given in units of voltage (50 mV/Div), and the abscissa is the time after mixing (0.1 s/Div). Syringe *A* contained DMPC vesicles (0.06 mg/ml) that were prepared in 2.3×10^{-4} M calcium and diluted to their final concentration (0.06 mg/ml) in 0.1 M Hepes, pH 7.06; syringe *B* contained 6.7×10^{-8} M A23187 in 0.01 M Hepes, pH 7.06. The temperature was maintained 34°C. The oscilloscope was set in the repetitive-sweep mode. The light-dark amplitude with water was 0.49 V. (*B*) A stopped-flow progress curve showing the effect of external calcium on the fluorescence time-course is presented. The ordinate is fluorescence intensity given in units of voltage (10 mV/Div), and the abscissa is the time after mixing (0.5 s/Div). Syringe *A* contained DMPC vesicles (0.06 mg/ml) in 0.01 M Hepes, pH 7.06; syringe *B* contained 6.2×10^{-8} M A23187, 10^{-4} M calcium in 0.01 M Hepes, pH 7.06. The temperature was maintained at 34°C. The oscilloscope was set in the repetitive sweep mode. The light-dark amplitude with water was 0.62 V.

occurred in our system. To show this the fluorescence of DMPC vesicles loaded with Ca^{2+} and CTC (chlorotetracycline) was monitored as a function of time as Ca-CTC left the vesicles ($t_{1/2} \simeq 1$ min.). Addition of A23187 caused the CTC fluorescence to drop (within the mixing time of the experiment, >3 s) to the same fluorescence value that was obtained when all the Ca^{2+} and CTC were uncomplexed. Furthermore, it was found that the fluorescence of A23187 at equilibrium was the same as when no Ca^{2+} was present. These experiments indicate that the A23187 and its Ca^{2+} complex rapidly cross the lipid membrane.

As discussed above (in Equilibrium Studies) the binding of A23187 to the membrane results in an increase in the ionophore's fluorescence, while the formation of a Ca^{2+}:ionophore complex quenches the fluorescence. These properties were used to study the transmembrane movement of $H^+ \cdot A23187^-$ and its cation complexes with rapid mixing techniques. Fig. 6 is a typical oscilloscope trace that is observed when A23187 is rapidly mixed with DMPC vesicles at pH 7.0 in the absence of divalent cations. The rapid fluorescence increase in Fig. 6 ($t_{1/2} \simeq$ 25 ms) might be associated with binding of the ionophore to the membrane, equilibration of the ionophore across the membrane, or both. We found that the half-time associated with this phase was not dependent on variations in ionophore concentration (3.3×10^{-6}–1.3×10^{-7} M at lipid concentrations of 0.03 mg/ml), and did not change when the lipid concentration was doubled (0.06 mg/ml). Figure 7*A* shows that when DMPC vesicles are loaded with Ca^{2+} and then mixed with A23187 and EDTA (used to complex any Ca^{2+} external to the vesicles), two exponential phases associated with the fluorescence rise can be seen. A biexponential computer fit to the data ($R^2 > 0.99$) indicates that the fast phase has the same time-course as the phase seen in Fig. 6, whereas the slower phase has a $t_{1/2}$ of ~0.3 s. The fast phase is due to the binding and equilibration of A23187 across the membrane as in Fig. 6. This indicates that the rate constant for transport of the protonated ionophore (k' in Fig. 1) is $\geq 28\ s^{-1}$. The slower phase is due to some of the ionophore complexing with the Ca^{2+} and transporting it out of the vesicles. Since the Ca^{2+} transported from the vesicles is complexed with the EDTA it is no longer available to quench the A23187 and the uncomplexed ionophore will now be able to contribute to the fluorescence rise. The sum of the amplitudes associated with the fast fluorescence rise and slow fluorescence rise in Fig. 7*A* is the same as the total fluorescence rise in Fig. 6, which indicates that all the Ca^{2+} was removed from the Ca^{2+}-loaded vesicles. If our interpretation of the slow phase of fluorescence rise as being associated with the transport of Ca^{2+} is correct, an experiment in which vesicles were "jumped" with both the ionophore and Ca^{2+} would produce a rapid phase associatd with ionophore transmembrane equilibration, followed by a slower quenching phase associated with equilibrium of the Ca^{2+}:ionophore complex across the membrane. In Fig. 7*B* such a result is found ($t_{1/2} \simeq 0.9$ s for the quenching phase and $t_{1/2} \simeq 25$ ms for the fast phase).

If the binding of A23187 and its cation complexes were rate limiting then both the fast and slow phases should be multiexponential. A computer fit of each phase in Figs. 6 and 7 indicated that both the fast and slow phases were well fit by a single exponential ($R^2 > 0.997$). Attempts to fit the data with additional exponentials indicated that their amplitudes were not significantly different from zero. This is consistent with the fact that equilibration between the aqueous phase and the membrane is rapid when compared with the translocation of A23187 and its complexes across the membrane, as shown in Fig. 1.

The following experimental design eliminates the fast phase and reports the transport of the

Ca^{2+}:ionophore complex directly. This is accomplished by preequilibrating the vesicles with both Ca^{2+} and A23187 and then monitoring the changes in fluorescence after mixing with EDTA. We shall refer to this protocol as the Ca^{2+} efflux method. The monoexponential form of the fluorescence rise when this method is followed is displayed in the oscilloscope trace of Fig. 8*A*. We shall refer to the fluorescence amplitude of Fig. 8*A* as the slow fluorescence amplitude. The instantaneous fluorescence amplitude is determined by the difference between the total fluorescence amplitude ($\Delta Fl_T = Fl|_{Ca=0} - Fl|_{Ca=\infty}$) and the slow fluorescence amplitude. The experimental protocol used in the Ca^{2+} efflux method was followed for the remaining experiments in the paper, unless otherwise stated. In all the kinetic experiments the membrane concentration has been chosen so that the ionophore is virtually all membrane bound.

EFFECT OF $[Ca^{2+}]$ AND $[A23187]_T$ ON THE KINETICS OF Ca^{2+} EFFLUX The single phase behavior seen in Fig. 8*A* is typical of low Ca^{2+}-to-ionophore ratios ($[Ca]^i_T/[A23187]_T < 1$) and is a result of a single turnover (st) (or less) of the ionophore in order to move all the Ca^{2+} from the vesicles. We shall refer to the rate constant associated with this phase as the apparent rate constant, k_{app}. The value of k_{app} is a close approximation to the ionophore's turnover number since the transmembrane step of $H^+ \cdot A23187^-$ is rapid. If the Ca^{2+} concentration in the vesicles is raised ($[Ca]^i_T/[A23187]_T > 1.0$), it becomes necessary for the ionophore to turn over a number of times (recycle) in order to remove all the Ca^{2+} from the vesicles. In such a case we would expect the rise in fluorescence (st) to be delayed by the continual quenching of the ionophore by the excess Ca^{2+}. Figure 8*B* shows an oscilloscope trace produced under high Ca^{2+} conditions. A lag period precedes a phase in which the fluorescence rises. We shall refer to the time period for which the lag phase persists as the lag time. The apparent rate constant

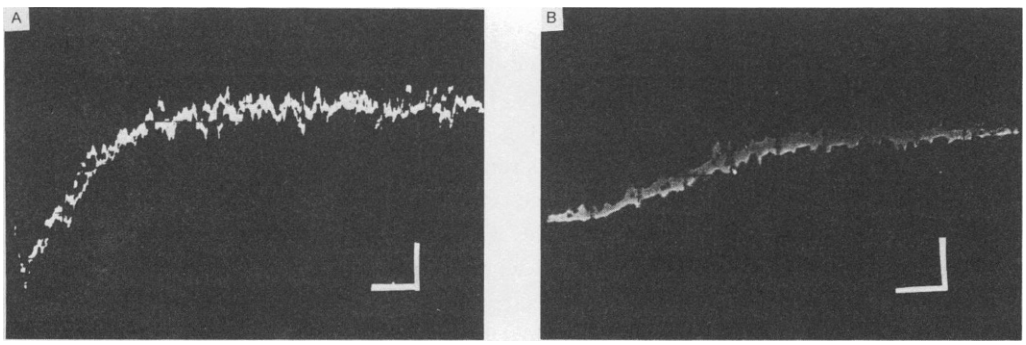

FIGURE 8 (*A*) A stopped-flow progress curve showing an oscilloscope trace using the Ca^{2+} efflux method at 34°C, pH 7.06, is presented. The ordinate is the fluorescence intensity given in units of voltage (20 mV/Div), and the abscissa in time after mixing (0.5 s/Div). Syringe *A* contained DMPC vesicles (0.06 mg/ml) preequilibrated with 1.3×10^{-7} M A23187 and 3.3×10^{-4} M Ca^{2+}; syringe *B* contained 0.1 M EDTA. All solutions were buffered with 0.05 M Hepes. The light-dark amplitude in water was 0.88 V. (*B*) A stopped-flow progress curve showing an oscilloscope trace using the Ca^{2+} efflux method at high Ca^{2+} concentrations is presented (34°C, pH 7.06). The ordinate is the fluorescence intensity given in units of voltage (20 mV/Div), and the abscissa in time after mixing (2 s/Div). Syringe *A* contained DMPC vesicles (0.06 mg/ml) preequilibrated with 6.7×10^{-8} M A23187 and 1.6×10^{-3} M Ca^{2+}; Syringe *B* contained 0.1 M EDTA. All solutions were buffered with 0.05 M Hepes. The light-dark amplitude in water was 0.51 V.

k_{app} will be associated with the fluorescence rise phase. Calcium efflux experiments using Ca^{2+} concentrations of 1.02 mM ($[Ca]_T^i/[A23187]_T = 1.09$)[2] and 1.7 mM ($[Ca]_T^i/[A23187]_T = 1.49$) yield lag times of 3.4 and 4.3 s, respectively. With the experimentally determined rate constants of 0.36 and 0.31 s^{-1} (for $[Ca^{2+}]$ of 1.02 and 1.7 mM, respectively) the ionophore must turnover (k_{app} × time lag) 1.22 and 1.33 times, respectively. Since the high buffer concentration should hold the intravesicular H^+ concentration constant throughout the experiment, we expect that k_{app} will be the same at all Ca^{2+} concentrations. As seen in Fig. 9*A* this is true for all Ca^{2+} concentrations regardless of whether the fluorescence rise phase is preceded by a lag time. Figure 9*B* shows that the slow fluorescence amplitude increases with increasing Ca^{2+} concentrations in agreement with the equilibrium results (see Fig. 5).

DETERMINATION OF THE KINETIC CONSTANTS Analysis of Figs. 9*A* and 9*B* was facilitated by the fact that the aqueous reactions in Fig. 1 could be neglected since we were working at lipid and ionophore concentrations of 0.03 mg/ml and 6.7 × 10^{-8} M, respectively (i.e., virtually all the ionophore was membrane bound). Accordingly, Fig. 10 shows the simplified scheme of Fig. 1 used to study the kinetic data when the aqueous reactions are omitted. The equilibrium association constant for the formation of the 1:1 complex is K_1 and the equilibrium association constant for the formation of the 1:2 complex from the 1:1 complex is K_2. The equilibration of $H^+ \cdot A23187^-$ is taken to be instantaneous in Fig. 10, with equilibrium constant $K_0 = 1$. As shown in Figs. 6 and 7 this process is rapid compared with the Ca^{2+}:ionophore transport process. If pK_A^{app} is fixed at −7.26 (determined from Fig. 4), the three parameters (K_1, K_2, and k) should be capable of describing Figs. 9*A* and 9*B* and the kinetic curves produced by the Ca^{2+} efflux method. It is important to recognize that the lag time seen at high Ca^{2+} concentrations is not a fit parameter. The kinetic treatment that

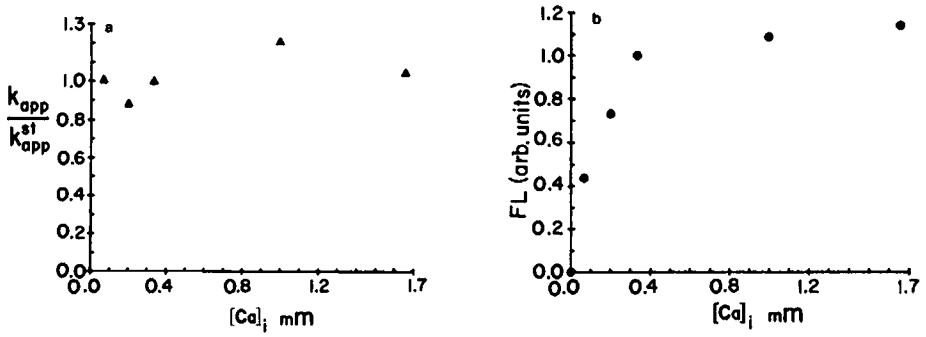

FIGURE 9 (*A*) the k_{app} normalized to the k_{app}^{st} (k_{app}/k_{app}^{st}) is plotted against internal free Ca^{2+}. The lipid concentration (DMPC) was 0.06 mg/ml and ionophore concentration of 6.7 × 10^{-8} M A23187. The protocol followed was according to the Ca^{2+} efflux method (at 34°C, pH 7.06). The rates were normalized to that for a Ca^{2+} concentration of 3.3 × 10^{-4} M (k_{app}^{st} = 0.51 ± 0.22s^{-1}). (*B*) The slow fluorescence amplitude (normalized to 1.0 at $[Ca^{2+}]$ of 3.3 × 10^{-4} M) is shown vs. free Ca^{2+} concentrations. The experimental points are for the same experiments in Fig. 9*A*.

[2]The total internal Ca^{2+} (bound plus free) is calculated by assuming a vesicular radius of ~120 Å and ~10^4 lipids/vesicle (15). To the free internal vesicular Ca^{2+} (= [Ca] × vesicular volume) is added half the membrane-bound Ca^{2+} (ionophore bound) calculated from Eq. 7, with K_1 = 1.5 × 10^5 M^{-1} and pK_A^{app} = −7.26, to obtain the total internal Ca^{2+} (in moles). For lipid concentrations used, A23187 was virtually all in the membrane.

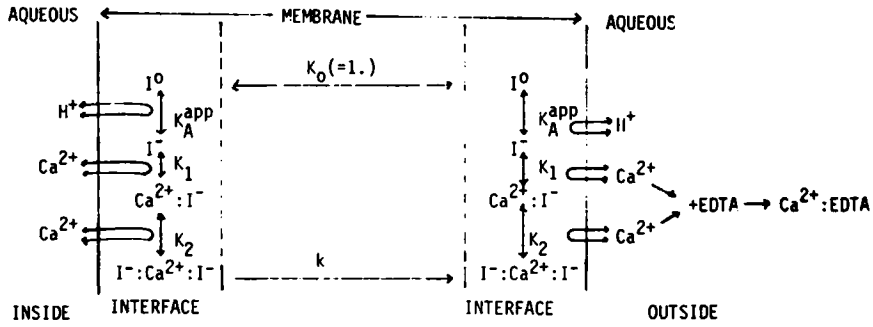

FIGURE 10 A simplified transport scheme for the calcium efflux method is shown. "*I*" represents the ionophore; the equilibrium association constants (K_1, K_2, K_o) and rate constants (k) are shown in the scheme.

follows, describing Fig. 10, is capable of predicting this phenomenon. As shown in the Appendix, the two coupled equations that determine the time-course of A23187 are the conservation equation for A23187,

$$[A_T] = 2 \cdot (1 + [H^+]K_A^{app}) \cdot ([A_i(t)] + \{K_1[A_i(t)] + 2K_1K_2[A_i(t)]^2[Ca_T^i(t)]\}/ \{1 + K_1[A_i(t)] + K_1K_2[A_i(t)]^2\}), \quad (8)$$

and the kinetic equation for Ca^{2+},

$$\frac{d[Ca_T^i(t)]}{dt} = -\{kK_1K_2[A_i(t)]^2[Ca_T^i(t)]\}/\{1 + K_1[A_i(t)] + K_1K_2[A_i(t)]^2\}, \quad (9)$$

where $[A_T]$ and $[A_i(t)]$ are the total and negative inner membrane free ionophore (at time t), $Ca_T^i(t)$ is the total vesicular Ca^{2+} (at time t), K_A^{app} is the apparent association constant (~ -7.26; see Fig. 4), and K_1, K_2, and k are the equilibrium and rate constants shown in Fig. 10. The apparent rate constant (k_{app}), measured by the fluorescence rise, is obtained by differentiating Eq. 8 with respect to time. As shown in the Appendix it is in general a complicated function of equilibrium and rate constants. For small ionophore concentrations ($K_1 \cdot A_T < 1$), however, the apparent rate constant will be proportional to K_1, K_2 and k. Eq. 8 was used to fit Fig. 9*B*, which results in $K_1 \leq 4.64 \times 10^4\ M^{-1}$ and K_2 found to lie between 3.0×10^{-4} and 3.1×10^{-3} (ionophore [mole]/lipid [mole]; $K_1/K_2 \sim 200$). The discrepancy between the K_1 value obtained kinetically ($4.6 \times 10^4\ M^{-1}$) and by equilibrium methods ($1.5 \times 10^5\ M^{-1}$) is attributed to variations in the amplitude data (10%) and to the fact that the theoretical fit to Fig. 9*B* used the equilibrium value of K_1 (see Appendix). In Fig. 11*A* the fluorescence curves calculated from Eqs. 8 and 9 are shown. At high $[Ca^{2+}]$ the theory predicts the existence of fluorescence lag times. Fig. 11*B* shows the theoretical fits of two experimental curves. It is clear that the theory provides a good representation of the data. The experimental ratio of the instantaneous fluorescence amplitude ΔFl_T at Ca^{2+} concentrations of 3.3×10^{-4} M is 0.33; this ratio is seen to be ~0.34 in Fig. 11*A*. The slow fluorescence amplitude can be >50% of the total amplitude because of the rapid equilibration of $H^+ \cdot A23187^-$ after the Ca^{2+} has been removed with the EDTA. To obtain an apparent rate constant (k_{app}) of ~0.6 s^{-1}, in Fig. 11*A*, the rate constant k for the 1:2 complex crossing (see

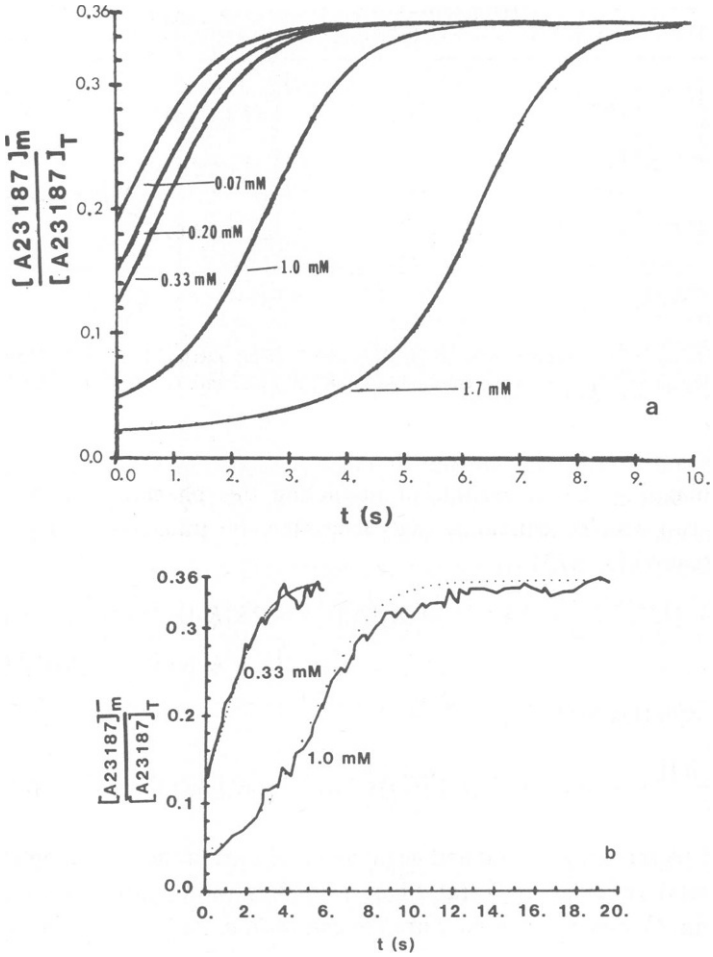

FIGURE 11 (*a*)The theoretical curves for fluorescence vs. time are shown for different Ca^{2+} concentrations. The ordinate is the amount of membrane bound negative ionophore to total ionophore. This quantity is proportional to the fluorescence. The experimental conditions used in Fig. 9 were simulated by Eqs. 8 and 9 in the text, along with the experimental concentrations (see Appendix). We took $K_1 = 4.65 \times 10^4$ M^{-1}, $K_2 = 3.2 \times 10^{-4}$, $k = 0.1$ s^{-1}, and $pK_A = -7.26$. (*b*) Two experimental traces were fit (by eye) according to the theory (dotted lines) developed in the text. At $[Ca^{2+}] = 0.33$ mM, the fit parameters were $k = 0.13$ s^{-1}, $K_1 = 4.65 \times 10^4$ M^{-1}, $K_2 = 3.2 \times 10^{-4}$ (mol/mol); and for $[Ca^{2+}] = 1.0$ mM the fit parameters were $k = 0.33$ s^{-1}, $K_1 = 4.65 \times 10^4$ M^{-1}, $K_2 = 6 \times 10^{-4}$ (mol/mol) [A23187] $= 6.7 \times 10^{-8}$ M.

Fig. 10) was taken to be 0.1 s^{-1} (0.3 s^{-1} for $K_2 = 3.1 \times 10^{-3}$). Studies on Ca^{2+} transport using X537A (8) indicate that the transport of Ca^{2+}:$X537A_2^-$ is rapid ($k_{ca:x_2} \geq 35$ s^{-1}) compared with that of the neutral Ca^{2+}:A23187 complex. In Table III we show the variations in k_{app} as a function of A23187 at a fixed Ca^{2+} concentration. The experimental variation of k_{app} with ionophore concentration indicates a quadratic dependence at low ionophore concentrations. Theoretically, this is true at only small ionophore concentrations ($<10^{-7}$ M), reaching a constant value equal to k (see Appendix) at high concentrations ($A_T^2 \gg 1/K_1K_2$). At

TABLE III
APPARENT RATE CONSTANT (k_{APP}) AS A FUNCTION OF $A23187_T$

$[A23187]_T \times 10^{-8}$	k_{app}	$[Ca^i_{free}]/[A23187]_T$	$[Ca_{Bound}]/[A23187]_T$	$[Ca^i_T]/[A23187]_T$	$k^{theo,A}_{app}$	$k^{theo,B}_{app}$
	(s^{-1})				(s^{-1})	(s^{-1})
6.7	0.51 ± 0.22	0.192	0.482	0.674	0.6	0.6
13.3	1.73 ± 0.37	0.096	0.482	0.578	2.9	2.04
20.0	4.23 ± 0.6	0.064	0.482	0.546	4.98	2.46

Ionophore concentrations are those before mixing. The Ca^{2+} concentration was fixed at 3.3×10^{-4} M (before mixing); lipid concentration (before mixing) = 0.06 mg/ml. The third and fourth columns are the molar ratios of free vesicular calcium and of bound vesicular calcium, respectively, to ionophore. The fifth column represents the quantity used in the theoretical calculation. The apparent rate constants are given in the sixth and seventh columns calculated for (*A*) $K_2 = 3.1 \times 10^{-3}$ and (*B*) $K_2 = 3.02 \times 10^{-4}$.

concentrations where A_T (total amount of ionophore) is approximately equal to $1/K_1$ the apparent rate constant (k_{app}) is primarily determined by the product of K_2 and k. Such a sensitive dependence on K_2 is demonstrated in Table III. The experimental values of k_{app} in Table III are found to be in the theoretically predicted range. It is important to note that if a 1:1 transport scheme were used to fit Figs. 9*A* and *B*, agreement with the experimental values of k_{app} as a function of ionophore concentration (Table III) would be poor.

EFFECT OF X537A ON LAG TIME The ionophore X537A is capable of transporting Ca^{2+} and decreasing the lag time observed with A23187. Experiments were carried out to

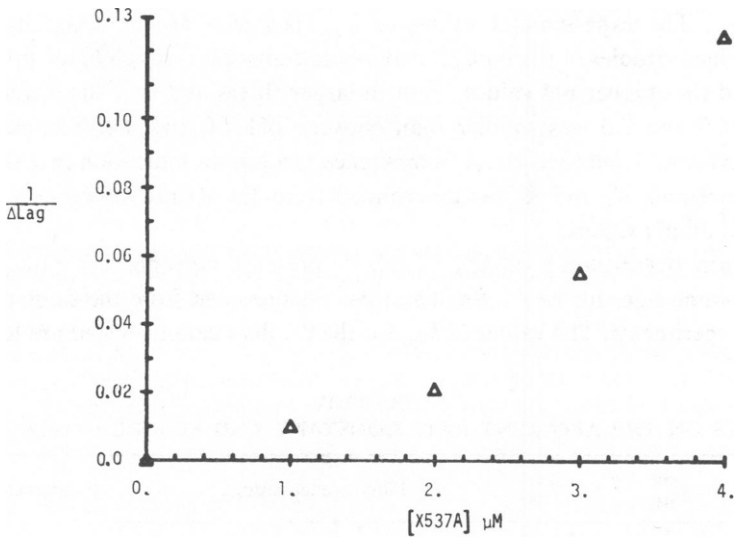

FIGURE 12 Effect of X537A concentration on the rate of Ca^{2+} release from PC vesicles at 30°C. Experiments were performed in the configuration of Fig. 8*B*, except that X537A was present in both reservoirs at the concentration indicated. The vesicles were loaded with 5 mM Ca^{2+} and efflux was initiated by mixing 7.5 mM EDTA. The DMPC and A23187 concentrations after mixing were 8.2×10^{-5} and 3×10^{-8} M, respectively. The standard medium contained 25 mM KCl and 50 mM Hepes buffer, pH 7.1. The rate was calculated as $[(\text{lag time}_x)^{-1} - (\text{lag time})^{-1}]$ where X represents the presence of X537A.

determine the rate of Ca^{2+} transport by X537A, using the effect on the lag time reported by a low concentration of A23187. The rate of Ca^{2+} transport is proportional to the increase in the reciprocal lag time, Δ (1/lagtime). Fig. 12 shows that this quantity increases with increasing [X537A]. The figure shows upward curvature indicating a greater than first-power dependence, in keeping with a 1:2 stoichiometry of the transport species (8). The relative rates of $Ca(A23187)_2$ transport and $Ca(X537A)_2$ transport were determined by comparison of the concentrations of the two ionophores necessary to give rise to the same increment in rate. When the control experiment was repeated with 6×10^{-8} M A23187, an absolute value of $(lagtime)^{-1}$ of 0.14 s^{-1} was observed. This is close to the value observed when catalyzed by 4×10^{-6} M X537A. Under these conditions A23187 is 67 times more effective than X537A in transporting Ca^{2+}, in agreement with the findings of Hyono et al. (14) and Caswell and Pressman (6). Under these conditions >50% of both ionophores were membrane bound (cf. 8) and the A23187 was operating in the nonlinear portion of its 1/lagtime vs. [ionophore] graph. The difference in efficiency is almost entirely due to the difference in efficiency in making of the 1:2 complex (i.e., differences in the K_2 values).

pH DEPENDENCE OF k_{APP} In Table IV we show the effect of pH on k_{app} and the fluorescence amplitude. The apparent rate constant (k_{app}) increases with higher pH while the fluorescence ratio is reduced. Theoretical k_{app} values were calculated according to the transport theory described in the Appendix. Theoretical values show the same trend as the experimental values (Table IV). The higher rates with increasing pH follow from the fact that more $A23187^-$ is available for transport at higher pH values. The lower fluorescence ratios (smaller instantaneous fluorescence to total fluorescence) at higher pH values are consistent with this interpretation since $A23187^-$ has a lower fluorescence quantum yield than $H^+ \cdot A23187^-$. The experimental values of k_{app}, however, are in disagreement with the theoretical values. Studies of pH on Ca^{2+}:ionophore transport through black lipid membranes (4) also found that higher pH values result in larger fluxes and that the difference between rates at pH 6.0 and 7.0 was smaller than between pH 7.0 and 8.0. The close agreement between experimental and theoretical fluorescence ratios is an indication that the equilibrium association constants K_1 and K_2 (as determined from Eq. 8) are adequate to describe the equilibrium at all pH values.

CATION DEPENDENCE OF k_{APP} Table V presents the apparent rate constants and fluorescence amplitudes for Mg^{2+}, Sr^{2+}, and Ba^{2+} determined from the same protocol as the Ca^{2+} efflux experiments. The values of k_{app} for the divalent cations tested are lower than that

TABLE IV
pH EFFECTS ON THE APPARENT RATE CONSTANT AND FLUORESCENCE AMPLITUDE

pH	k_{app}^{exp}	k_{app}^{theo}	Fluorescence $ratio_{exp}$	Fluorescence $ratio_{theo}$
	(s^{-1})	(s^{-1})		
6.0	0.32	0.06	0.4	0.42
7.0	0.51	0.67	0.4	0.31
7.6	2.2	1.25	0.1	0.2

The errors in the experimental rate constants are ~10%. The errors in the Fluorescence ratios ($\Delta Fl_{inst}/\Delta Fl_T$) are ~20%. The final concentrations after mixing were [A23187] = 3.3×10^{-8} M, $[Ca^{2+}] = 1.7 \times 10^{-4}$, and lipid concentration was 0.03 mg/ml. The theoretical values were calculated as described in the Appendix.

TABLE V

THE DEPENDENCE OF APPARENT RATE CONSTANT AND FLUORESCENCE AMPLITUDE ON DIVALENT CATION

Cation	k_{app}/k^{st}_{app}	$\Delta Fl_{slow}/\Delta Fl^{st}_{slow}$
Ca^{2+}	1.0	1.0
Mg^{2+}	0.47	0.73
Sr^{2+}	0.031	0.57
Ba^{2+}	—	—

Both rate constant and slow fluorescence change have been normalized to the single turnover Ca^{2+} values ($k_{app} = 0.51 \pm 0.22\ s^{-1}$) and $\Delta Fl_{slow}/\Delta Fl_T = 0.55 \pm 0.08$). Final concentrations were $[M^{2+}] = 1.7 \times 10^{-4}$ M, $A23187_T = 3.3 \times 10^{-8}$ M and 0.03 mg/ml lipid (DMPC). The divalent cation concentrations used have been shown (see Figs. 9 and 10) not to saturate the ionophore. The apparent rate constants were found by fitting the data to a first-order process.

for Ca^{2+}. Furthermore, the decreasing k_{app} sequence for the divalent cations is identical with the affinity sequence of K_1 values found in the equilibrium section ($Ca^{2+} > Mg^{2+} > Sr^{2+} > Ba^{2+}$). These results are in keeping with the result that for low ionophore concentrations ($<10^{-7}$ M) k_{app} is proportional to K_1. Furthermore, as K_1 (the equilibrium association constant for formation of the 1:1 complex) is decreased, the amount of ionophore in the bound nonfluorescing form decreases, giving rise to the expectation that the slow fluorescence amplitude will decrease according to the affinity sequence. The third column in Table V indicates this is true. Variation of the Na^+ concentration (up to $[Na^+]/[Ca^{2+}] \sim 50$) produced no changes in the Ca^{2+} transport rates. When no Ca^{2+} was present, 10 mM Na^+ produced no fluorescence changes upon mixing, which indicates no transport. These results

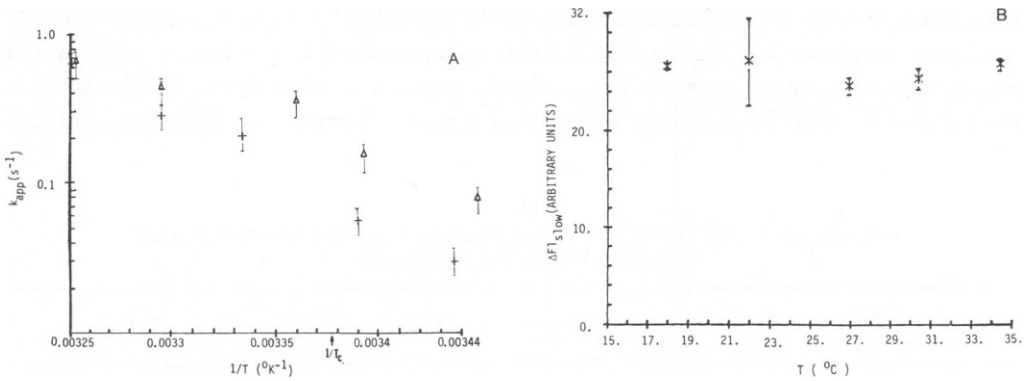

FIGURE 13 (*A*) k_{app} (log scale) is plotted against $1/t$. The plus signs (+) are a temperature run according to the Ca^{2+} efflux method. The triangles [Δ] are from an experimental similar to that in Fig. 7 *B*, where the A23187 was preequilibrated with vesicles. Both experiments contained final concentrations of lipid at 0.03 mg/ml and ionophore at 3.3×10^{-8} M. The final Ca^{2+} concentration was 1.7×10^{-4} M for the Ca^{2+} efflux method and 5.1×10^{-4} M for the other experiment. The pH was maintained at 7.06. A straight line fit for + gave a slope of 33 kcal/mol, whereas for Δ we found 22 kcal/mol. The errors indicate the lines are not significantly different. Analysis of covariance for the different experiments indicated that the slopes of the curves were not significantly different ($P > 0.05$); $n = 4$ for each datum point. (*B*) The slow fluorescence amplitude is plotted against temperature for the Ca^{2+} efflux experiment (+) in Fig. 13*A*. The total fluorescence amplitude was 50 U.

are in accord with our equilibrium experiments and previous experimental work (5) that showed A23187 binds monovalent cations weakly.

TEMPERATURE DEPENDENCE OF k_{APP} Fig. 13 *A* is an Arrhenius plot of k_{app} for Ca^{2+}:ionophore transport in DMPC membranes. A straight line fit to Fig. 13 *A* yields an activation enthalpy of 27.0 ± 6.0 kcal/mol. The linearity of Fig. 13 *A* over a temperature range that includes the phase transition temperature (~23°C for DMPC [16]) shows that dramatic changes in the fluidity of the system do not affect transport. There are two possible explanations for such a result: (*a*) the ionophore fits in both lipid phases (crystalline and gel) equally well, or (*b*) it disrupts its local environment (13) and thus is less sensitive to gross structural changes in the membrane. Recalling that k_{app} is approximately proportional to k_1, K_1 and K_2 ($A23187_T < 10^{-7}$ M) we expect that temperature variations in these constants determine the changes in the rates of transport. As demonstrated in earlier sections the slow fluorescence amplitude reflects the values of both K_1 and K_2 (see, for example, Eq. 8). Fig. 13 *B* shows that the slow fluorescence amplitude is unaffected by changes in temperature. We take this independence of temperature of the fluorescence amplitudes (Fig. 13 *B*) to be an indication that K_1 is independent of temperature since the slow fluorescence amplitude is more sensitive to changes in K_1 than K_2. The data are not complete enough to determine whether the continuous decrease of k_{app} in the Arrehenius plot is due to the k (the rate constant of the 1:2 complex), or to compensatory changes in k and K_2. Calcium transport using X537A, studied as a function of temperature, has indicated a break in the Arrhenius plot at the membrane phase transition temperature in both SR (17) and model membranes (8).

DEPENDENCE OF k_{APP} ON LIPID COMPOSITION Ca^{2+}:ionophore transport was studied in mixed lipid vesicles according to the Ca^{2+} efflux protocol. In Table VI the apparent rate constant (k_{app}) decreased relative to that of the pure DMPC vesicles for all mixtures used. The change in k_{app} could be due to changes in the fluidity of the membrane, head group interactions, or both. For vesicles containing DPPC and DMPE we expect the fluidity of the membrane to be lower (i.e., higher than T_c [18]) than pure DMPC membranes, which would thereby contribute to the decrease in k_{app}. Furthermore, in DMPC/DPPC membranes it is possible that the polar heads do not lie in the same plane (19) because of differences in acyl

TABLE VI
EFFECT OF LIPID MIXTURES ON APPARENT RATE CONSTANT AND FLUORESCENCE AMPLITUDE

Lipid mixture	k_{app}	$\Delta Fl_T/\Delta Fl_T^{\alpha}$	$\Delta Fl_{slow}/\lvert\Delta Fl_T\rvert$
	(s^{-1})		
DMPC	0.98	1.0	0.39 ± 0.04
DMPC/DPPC (32%)	0.019	1.31	0.50 ± 0.01
DMPC/DMPE (33%)	0.217	0.67	0.67 ± 0.002
DMPC/PA (31%)	0.057	−0.77	0.11 ± 0.02

The percentage values shown in the first column are the mol % (mol/100 mol) of lipid mixed with DMPC. The rate constants and ratio of total fluorescence amplitudes are accurate to better than 10%. The total fluorescence amplitudes are normalized to that for pure DMPC (260 mV); the negative sign for DMPC/PA indicates a higher fluorescence when there is Ca^{2+} (see text) than not. The Ca^{2+} efflux protocol was used with final concentrations of ionophore, Ca^{2+}, and lipid being 6.7×10^{-8} M, 1.7×10^{-4} M, and 0.03 mg/ml, respectively.

chain length of different lipids. Such an effect might allow more interaction between the ionophore and the polar head of the lipid, and thereby act to decrease k_{app} by making less membrane A23187 available for complexation and to increase the total fluorescence (relative to the pure DMPC vesicles), as shown in Table VI. In the DMPC/DMPE vesicles the fluidity of the hydrophobic region is less than in the pure DMPC vesicles. This effect, however, is produced by the different head group interactions. PE tends to tighten up the membrane (i.e., it produces a smaller area per lipid head than PC, [20]) and may act to exclude the ionophore from the polar group head region giving rise to a decrease in the total fluorescence relative to pure DMPC vesicles, and a relative decrease in k_{app}. It is possible that $A23187^-$ binding with the PE could also produce the decrease in total fluorescence and k_{app}. The decrease in k_{app} in DMPC/PA^- mixed vesicles cannot be attributed to fluidity effects in the hydrophobic region, since PA^- would tend to make this region more fluid than DMPC vesicles. The decrease in k_{app} can be explained if one considers the fluorescence results in Table VI. The minus sign for the total fluorescence amplitude indicates that the fluorescence is greater when Ca^{2+} is in the system. From our equilibrium studies we have found that the fluorescence of A23187 is predominantly quenched by the Ca^{2+}:ionophore complex in a 1:1 stoichiometry for DMPC vesicles. A 1:1 complex existing in DMPC/PA^- vesicles might tend to form a ternary $A23187^-$-CA^{2+}-PA^- complex that would restrict the A23187 motion and possibly enhance fluorescence. Furthermore, this binding would reduce the amount of ionophore available for transport and thus reduce k_{app}. We were not able to resolve Ca^{2+} transport in DMPC/PS^- vesicles. This could be due to the difference in the PA^- and PS^- headgroups and to the ability of the 1:1 complex to partition in the membrane. In all cases we found that the final fluorescence amplitude was the same after Ca^{2+} removal. The binding properties of X537A also seem to be affected by the nature of the polar head group (8). It has been demonstrated that changes in k_{app}, although slightly affected by changes in the membrane fluidity (previous section), are dominated by interactions of the Ca^{2+}:ionophore complex with the polar head region of the lipids.

DETERMINANTS OF TRANSPORT EFFICIENCY In the present study we have quantitated the elementary steps in the cycle by which A23187 achieves $Ca^{2+}/2H^+$ exchange across

TABLE VII
SUMMARY OF EQUILIBRIUM AND KINETIC CONSTANTS FOR THE A23187 TRANSPORT PROCESS

Process	Constant	Value
Membrane binding constant for the neutral species ($H^+ \cdot A^-$)	K_m^0	$4.9 \times 10^4\ M^{-1}$
Membrane binding constant for the negative species (A^{-1})	K_m^-	$6.61 \times 10^3\ M^{-1}$
Membrane binding constant for the 1:1 calcium ionophore specie ($Ca^{2+} \cdot A^-$)	$K_{1,B}$	$\sim 6.6 \times 10^3\ M^{-1}$
Association constant of H^+ with membrane-bound A^-	pK_A^m	-7.55
Association constant of H^+ with aqueous A^-	pK_A	-6.68
Association constant of Ca^{2+} with membrane bound A^- to membrane-bound $Ca^{2+} \cdot A^-$	K_1	$4.6 \times 10^4\ M^{-1}$
Association constant for the formation of the 1:2 complex from the 1:1 complex in the membrane	K_2	$(0.3 - 3.1) \times 10^{-3}$ (ionophore/lipid mole)
Rate constant for transport for the $(Ca^{2+} \cdot A^-)_2$ complex	k	$0.1 - 0.3\ s^{-1}$
Rate constant for transport for the $H^+ \cdot A^-$	k'	$\geq 28\ s^{-1}$

membranes. The equilibrium and kinetic constants of the individual steps of the transport cycle (Fig. 1) are summarized in Table VII. The interfacial reactions are so rapid that they were not resolved in our stopped-flow experiments. The transport reactions were resolved. Transport of the protonated form of the ionophore is more rapid than transport of the $Ca^{2+} \cdot A^-)_2$ form. The overall $Ca^{2+}/2H^+$ exchange rate at any particular ionophore concentrations is limited by the rate of transport of the $Ca^{2+} \cdot A^-)_2$ complex, whose concentration is determined by the Ca^{2+} concentration and total ionophore concentration. At the A23187 concentrations used here and in most biological experiments, the rate of divalent cation transport is a sensitive function of the product of $K_2 \cdot [A23187^-]$ and k (Table III). The mechanism of A23187-mediated transport is analogous to that of X537A, which performs $Ca^{2+}/2K^+$ exchange by a similar mechanism. The 67-fold efficacy of Ca^{2+} transport by A23187 compared with that of X537A is attributed to the greater ability of A23187 to form the 1:2 complex. However, it seems that this advantage is partially offset by a lower k value (0.1–0.3 s^{-1} for A23187 vs. $\geq 35\ s^{-1}$ for X537A), which indicates that the A23187 complexes cross the membrane less rapidly than the X537A complexes. This effect may be explained by an enhanced lipid-ionophore interaction, which is supported by the fact that A23187 partitions ~10-fold more strongly in the membrane than X537A.

The divalent cation specificity of A23187 transport can be explained largely on the basis of the affinity for 1:1 complexation. The values of k_{app} for the various complexes (Table V) closely parallel the K_1 values (Table II), which indicates that the product of K_2 and k is relatively indifferent to the type of divalent cation complexed.

The rate of transport by A23187 is sensitive to the lipid composition of the membrane. The ionophore and its complexes partition in the head group region of the membrane and are sensitive to the head group composition. PA^- or PE addition results in a decrease in the transport rate. Similar results were observed with X537A (8). Our results may be explained by binding of the $Ca^{2+} \cdot A23187^-$ and $A23187^-$ complexes to the PA^- or PE head groups, respectively. The elucidation of interaction between the ionophore and lipid molecules in its immediate vicinity remains an important problem in the prediction of transport efficiency.

APPENDIX

Kinetic Theory of Transport of Ca^{2+} with A23187

The mechanism of transport of divalent cations across phospholipid bilayers is treated theoretically according to the scheme in Fig. 10.

At any time t, the total amount of A23187 (A_T) is a conserved quantity given by the equation

$$A_T = A_i(t) + A_i^0(t) + A_o(t) + A_o^0(t) + 2K_1K_2\,Ca_i\,A_i^2(t) + 2K_1K_2\,Ca_o(t)\,A_o^2(t) + K_1\,A_i(t)\,Ca_i(t) + K_1\,A_o(t)\,Ca_o(t), \quad \text{(A1)}$$

where concentration brackets have been suppressed,the superscript "0" represents the neutral form of the ionophore (no superscript is written for negative forms) and the subscripts "i" and "o" refer to the inside and outside membrane surface, respectively. The binding constants K_1 and K_2 are defined by the following equations:

$$K_1 \equiv \frac{[CaA]_{i,o}}{[Ca]_{i,o}[A]_{i,o}} \quad \text{(A2)}$$

$$K_2 \equiv \frac{[CaA_2]_{i,o}}{[CaA]_{i,o}[A]_{i,o}} \tag{A3}$$

The total internal calcium (Ca_T^i) is similarly given by

$$Ca_T^i(t) = Ca_i(t) + K_1\,Ca_i(t)\,A_i(t) + K_1K_2\,Ca_i(t)\,A_i^2(t). \tag{A4}$$

Unlike Eq. A1, however, the total internal calcium changes as a function of time. To calculate this change we recognize that for small intervals of time Δt ($\Delta t \ll 1/k$), the change in total internal calcium is given by

$$Ca_T^i(t + \Delta t) = Ca_T^i(t) - k\Delta t\,[CaA_2^i(t)]. \tag{A5}$$

Eliminating $CaA_2^i(t)$ in Eq. A5 by using Eqs. A2–4 we find

$$Ca_T^i(t + \Delta t) = Ca_T^i(t)\left\{1 - \frac{\Delta t k K_1K_2A_i^2(t)}{[1 + K_1A_i(t) + K_1K_2A_i^2(t)]}\right\}. \tag{A6}$$

From the change in Ca_T^i we can calculate how A_i changes with time from Eq. A1. One simplification is to assume that the equilibrium reactions are all fast compared with Δt, so that the two terms involving complexation of ionophore on the outside of the membrane can be neglected and any calcium moving across the membrane is rapidly complexed with the EDTA. These interfacial reactions are faster than 3 ms, as shown in the paper. Furthermore, we have shown experimentally that equilibration of the neutral form across the membrane is rapid ($A_o = A_i$). Within these approximations Eq. A1 reduces to

$$A_T = 2(1 + H^+K_A^{app})A_i(t + \Delta t) + (K_1A_i(t + \Delta t) + 2K_1K_2A_i^2(t + \Delta t)) \cdot Ca(t + \Delta t), \tag{A7}$$

where $A_i^0 \equiv K_A^{app}\,A_i \cdot H^+$ (with $K_A^{app} \sim -7.26$; see Fig. 4). Rewriting Eq. A7 in terms of Ca_T^i yields

$$A_T = 2(1 + H^+ \cdot K_A^{app})A_i(t + \Delta t) + \{[K_1A_i(t + \Delta t) + 2K_1K_2A_i^2(t + \Delta t)]Ca_T^i(t + \Delta t)\}/[1 + K_1A_i(t + \Delta t) + K_1K_2A_i^2(t + \Delta t)]. \tag{A8}$$

From Eqs. A6 and 8 we can completely determine the time-course for the fluorescence increase as a function of ionophore and calcium according to the following algorithm:

(*a*) Calculate the total number of moles of internal calcium. This is done by assuming a vesicular volume and calculating the free internal calcium and the bound internal calcium (before mixing) according to the equilibrium value of K_1. The two calcium values are added to give the total internal calcium. It should be noted that for total self-consistency the K_1 and K_2 values obtained in the next step should be used to recalculate the bound calcium in this step and this procedure iterated until the starting K_1 and K_2 values equal the final values within some desired error. This iteration was not carried out in our program and was certainly a source of error. We expect this error to be small since $K_2/K_1 \sim 10^{-2}$, which indicates that neglect of K_2 terms are reasonable.

(*b*) Fit Eq. A8 at time $t = 0$ to the slow fluorescence amplitudes to get K_1 and K_2.

(*c*) Using Eq. A6, generate $Ca_T^i\,(t + \Delta t)$ (using K_1, K_2 and an assumed value for k).

(*d*) Solve Eq. A8 self-consistently for $A_i\,(t + \Delta t)$.

(*e*) Repeat steps (*c*) and (*d*) increasing the time by Δt until the full fluorescence curve has been determined.

(*f*) Readjust k so that the theoretical apparent rate constant is the same as the experimental apparent rate constant.

The results of this procedure are shown in Fig. 11 of the paper.

Rate Equation for A23187

By differentiating Eq. A8 with respect to time we can calculate the kinetic equation for the change in negative ionophore. After much algebraic manipulation and the use of Eq. A6 to eliminate dCa_T^i/dt we find

$$\frac{dA_i(t)/dt}{A_i(t)} = \frac{(kK_1K_2)[K_1A_i^2(t) + 2K_1K_2A_i^3(t)]Ca_T^i(t)}{2(1 + H^+K_A^{app})[1 + K_1A_i(t) + K_1K_2A_i^2(t)]^2 + Ca_T^i(t)[K_1 + K_1^2K_2A_i^2(t) + K_1K_2A_i(t)]} . \quad \text{(A9)}$$

For small values of ionophore ($<10^{-7}$ M), terms involving K_2 in Eq. A9 are small; hence

$$dA_i(t)/dt \simeq \frac{kK_1K_2A_i(t)[K_1A_i^2(t)]Ca_T^i(t)}{2(1 + H^+K_A^{app})[1 + K_1A_i(t)]^2} .$$

The above equation can be rewritten with the aid of Eq. A6:

$$dA_i/dt \simeq -\frac{dCa_T^i/dt}{2(1 + H^+K_A^{app})} , \quad \text{(A10)}$$

where we have neglected 1 compared with K_1A (> 10). Therefore, for small calcium-to-ionophore ratios and small amounts of ionophore ($K_2\ A_i/K_1 < 1$), the rate of change of ionophore with time is proportional to the calcium flux. A prediction from Eq. A10 is that the proportionality constant is determined from K_A^{app}.

Finally we note that, as A_T gets very large ($K_1K_2A^2 > 1$), Eq. A6 goes to a simple first-order equation with rate constant k. As the ionophore concentration is decreased, Eq. A6 becomes second order in Ca_T^i ($K_1A > 1$ and $K_1K_2A^2 < 1$).

This work was supported by U. S. Public Health Service grants GM 07028, GM 23990, HL 07188, and HL 23392. The operation and continuing development of the PROPHET system is sponsored by the Chemical/Biological Information-Handling Program, Division of Research Resources, National Institutes of Health.

Received for publication 27 February 1980 and in revised form 20 February 1981.

REFERENCES

1. Reed, P. W., and H. A. Lardy. 1972. A23187: A divalent cation ionophore. *J. Biol. Chem.* 247:6970–6977.
2. Case, G. D., J. M. Vanderkooi, and A. Scarpa. 1974. Physical properties of biological membranes determined by the fluorescence of the calcium ionophore A23187. *Arch. Biochem. Biophys.* 162:174–185.
3. Deber, C. M., and D. R. Pfeiffer. 1976. Ionophore A23187: solution conformations of the calcium complex and free acid deduced from proton and carbon-13 nuclear magnetic resonance studies. *Biochemistry* 15:132–140.
4. Wulf, J., and W. G. Pohl. 1977. Calcium ion-flux across phosphatidylcholine membranes mediated by ionophore A23187. *Biochim Biophys. Acta.* 465:471–488.
5. Pfeiffer, D. R., P. W. Reed, and H. A. Lardy. 1974. Utraviolet and fluorescent spectral properties of the divalent cation ionophore A23187 and its metal ion complexes. *Biochemistry.* 13:4007–4014.
6. Caswell, A. H., and B. C. Pressman. 1972. Kinetics of transport of divalent cations across sarcoplasmic reticulum vesicles induced by ionophores. *Biochem. Biophys Res. Commun.* 49:292–298.
7. Anteunis, M. J. O. 1977. Solution conformation of the ionophore A23187 and its magnesium salt. *Bioorg. Chem.* 6:1–11.
8. Haynes, D. H., V. C. K. Chiu, and B. Watson. 1980. Study of the Ca^{2+} transport mechanism of X537A in phospholipid membranes using fluorescence and rapid mixing techniques. *Arch. Biochem. Biophys.* 203:73–89.

9. Chaberck, S., and A. Martell. 1959. Organic Sequestering Agents. John Wiley & Sons, New York.
10. Huang, C. 1969. Studies on phosphatidylcholine vesicles: formation and physical characteristics. *Biochemistry.* 8:344–350.
11. Litman, B. 1973. Lipid model membranes. Characterization of mixed phospholipid vesicles, *Biochemistry.* 12:2545–2554.
12. Puskin, J. S., A. Vistnes, and M. Coene. 1981. A Fluorescence study of A23187 interaction with phospholipid vesicles. *Arch. Biochem. Biophys.* 206:164–172.
13. Puskin, J. S., and T. E. Gunter. 1975. Election paramagnetic resonance of copper ion and manganese ion complexes with the ionophore A23187. *Biochemistry.* 14:187–191.
14. Hyono, A., T. Hendriks, F. J. M. Daemen, and S. L. Bonting. 1975. Movement of calcium through artificial lipid membranes and the effects of ionophores. *Biochim. Biophys. Acta.* 389:34–46.
15. Kolber, M. A., and D. H. Haynes. 1979. Evidence for a role of phosphatidyl ethanolamine as a modulator of membrane-membrane contact. *J. Membr. Biol.* 48:95–114.
16. Ladbrooke, B. D., and D. Chapman. 1969. Thermal analysis of lipid proteins and biological membranes. *Chem. Phys. Lipids.* 3:304–367.
17. Scarpa, A., J. Baldassare, and G. Inesi. 1972. The effect of calcium ionophores on fragmented sarcoplasmic reticulum. *J. Gen. Physiol.* 60:735–749.
18. Blume, A., and T. Ackermann. 1974. A Calorimetric study of the lipid phase transition in aqueous dispersions of phosphorylcholine-phosphorylethanolamine mixtures. *FEBS (Fed. Eur. Biochem. Soc.) Lett.* 43:71–74.
19. Jacobs, R. E., B. S. Hudson, and H. C. Andersen. 1977. A Theory of phase transitions and phase diagrams for one- and two-component phospholipid bilayers. *Biochemistry.* 16:4349–5459.
20. Lee, A. G. 1977. Lipid phase transitions and phase diagrams. I. Lipid phase transitions. *Biochim. Biophys. Acta.* 472:237–281.